Applied Energy 309 (2022) 118474

Contents lists available at ScienceDirect

Applied Energy

journal homepage: www.elsevier.com/locate/apenergy

Global energy assessment of the potential of photovoltaics for greenhouse farming

Eduardo F. Fernández [a,*], Antonio Villar-Fernández [a], Jesús Montes-Romero [a], Laura Ruiz-Torres [b,c], Pedro M. Rodrigo [a], Antonio J. Manzaneda [b,c], Florencia Almonacid [a]

[a] *Advances in Photovoltaic Technology (AdPVTech), CEACTEMA, University of Jaén (UJA), 23071 Jaén, Spain*
[b] *Departamento de Biología Animal, Biología Vegetal y Ecología, University de Jaén, 23071, Jaén, Spain*
[c] *Instituto Interuniversitario de Investigación del Sistema Tierra (IISTA), University of Jáen, 23071 Jaén, Spain*

HIGHLIGHTS

- The energy assessment of agrivoltaic (APV) systems is carried out.
- Representative locations with high density of greenhouses are considered.
- Important socioeconomic families of crops have been investigated.
- APV technology present average optimal transparencies of around 68%
- APV systems could produce up to 200 kWh/m^2 without affecting crops.

GRAPHICAL ABSTRACT

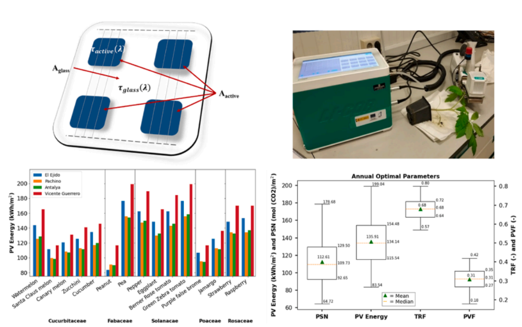

ARTICLE INFO

Keywords:
Photovoltaics
Agriculture
Energy assessment
Modelling
Systems
Agrivoltaics

ABSTRACT

Agrivoltaic (APV) systems have emerged as a promising solution to reduce the land-use competition between PV technology and agriculture. Despite its potential, APV is in a learning stage and it is still necessary to devote big efforts to investigate its actual potential and outdoor performance. This work is focused on the analysis of APV systems in agriculture greenhouses at global scale in terms of energy yield. To conduct this study, we introduce here a novel dual APV model, which is projected in four representative locations with a high crop cultivation greenhouse implantation, i.e. El Ejido (Spain), Pachino (Italy), Antalya (Turkey) and Vicente Guerrero (Mexico), and for 15 representative plant cultivars from 5 different important socioeconomic families of crops, i.e. Cucurbitaceae, Fabaceae, Solanacae, Poaceae, Rosaceae. At this stage, semi-transparent c-Si PV technology has been considered due its high efficiency and reliability. The results show that APV systems could have a transparency factor around 68% without significantly affecting the total crop photosynthetic rate. Taking this into account, APV systems would produce an average annual energy around 135 kWh/m^2, and values around 200 kWh/m^2 under a favourable scenario. This could represent a contribution to the total market share between 2.3% (México) and 6% (Turkey), and up to 100% of the consumption demand of greenhouses equipped with heating and cooling (GSHP), and lighting.

* Corresponding author.
E-mail address: eduardo.fernandez@ujaen.es (E.F. Fernández).

https://doi.org/10.1016/j.apenergy.2021.118474
Received 30 September 2021; Received in revised form 11 December 2021; Accepted 25 December 2021
Available online 10 January 2022
0306-2619/

Nomenclature

A	Area of the module, m^2
A_{max}	Maximum net photosynthesis rate, μmol CO2/m^2·s
AOI	Angle of incidence, °
AOIF	Angle of incidence factor, dimensionless
average TRF	Average transmittance factor of PV, dimensionless
c	Light speed, m/s
D	Direct tilted irradiance, W/m^2
DHI	Direct horizontal irradiance, W/m^2
Diff	Diffuse tilted irradiance, W/m^2
DiffHI	Diffuse horizontal irradiance, W/m^2
DNI	Direct Normal Irradiance, W/m^2
E	Spectral irradiance, W/(m^2·nm)
EQE	External Quantum Efficiency, dimensionless
F(AOI)	Angle of incidence modifier function, dimensionless
G	Global tilted irradiance, W/m^2
GHI	Global horizontal irradiance, W/m^2
h	Planck constant, eV·s
I	Component of irradiance to be scaled, W/m^2
L_{mod}	Potential internal losses of a PV module, dimensionless
MM	Spectral mismatch factor of crops, dimensionless
N_a	Avogadro constant, mol^{-1}
P/A	Power per unit area, W/m^2
PPFD	Photosynthetic photon flux density, μmol/m^2·s
PSN	Net photosynthesis rate, mol CO^2/m^2
PVF	Photovoltaic active factor, dimensionless
QY	Quantum Yield of plants, dimensionless
SF	Spectral factor of PV devices, dimensionless
SR	Spectral response, A/W
T	Temperature, °C
TF	Thermal factor, dimensionless
TRF	Spectral total transmittance factor, dimensionless
Z	Zenith angle, °

Greek symbols

γ	Temperature coefficient, $°C^{-1}$
β	Tilted angle of PV, °
η	Efficiency, dimensionless
λ	Wavelength, nm
ρ	Albedo coefficient, dimensionless.
τ	Spectral transmittance, dimensionless

Abbreviations

AM 1.5	Reference Air Mass
APV	Agrivoltaic
a-SI	Amorphous Silicon
B	Blue light
BSh	Arid, steppe, hot climate
BWk	Arid, desert, cold climate
CdTE	Cadmium Telluride
CIGS	Copper Indium Gallium Selenide
CO^2	Carbon Dioxide
CSa	Temperate, dry summer, hot summer climate
c-SI	Crystalline Silicon
DSSC	Dye sensitized solar cell
EU	European Union
FAO	Food and Agriculture Organization
GHGe	Greenhouse Gas Emissions
IPGC	International Panel for Global Change
K-G	Köppen-Geiger climate classification
LED	Light-emitting diode
NOCT	Nominal Operating Cell Temperature
OPV	Organic photovoltaic
PV	Photovoltaic
PVGIS	Photovoltaic Geographical Information System
R	Red light
SDGs	Sustainable Development Goals
SMARTS	Simple Model of the Atmospheric Radiative Transfer of Sunshine
STC	Standard Test Conditions
TMY	Typical Meteorological Year
UN	United Nations
USE	United States of America

Subscripts

"DH"	Direct horizontal irradiance
"DiffH"	Diffuse horizontal irradiance
"G"	Global tilted irradiance
"GRef"	Standard ASTM G173-03 global irradiance
"I"	Component of irradiance to be scaled
"Licor"	LI-COR light source
"SMARTS"	Spectral irradiance from SMARTS software
"plant"	Irradiance on plants
"STC"	Standard test conditions
"cell"	Solar cell
"mod"	PV module
"TPV"	Transparent photovoltaic module
"active"	Part of the module with active photovoltaic cells
"glass"	Part of the module with high transparent glass

1. Introduction

According to the last reports from the United Nations (UN) [1] and the International Panel for Global Change (IPGC) [2], if no actions are taken to reduce the greenhouse gas emissions (GHGe), global temperatures are about to increase between 1.5 °C and 3.2 °C by the end of the century. UN has come to an agreement on 17 Sustainable Development Goals (SDGs), in order to tackle this, and other environmental challenges of our age. Among those actions, the enhancement of renewable, sustainable and affordable energy is one of the main instruments to reduce atmospheric gas emissions. For instance, the production of energy is responsible of the 75% of greenhouse gas emissions in the EU [3].

Photovoltaic technology (PV) has positioned as the ideal source of energy to accomplish the goals of SDGs and the EU Green Deal in many countries due to its competitive price, flexibility and positive impact on job creation [4]. In this sense, at European Level, the expected increase of the installed capacity in the European Mediterranean Countries for the next ten years will be higher than 200 GW. However, the develop of PV may face at least two big challenges worldwide. First, the major need of space, coming in competence with land for agricultural uses, and second, the pressure on the so-called bad-lands which typically harbour high biodiversity [5]. Bearing this in mind, a solution must be found to avoid that the energy goals are met at the expense of biodiversity and food production, which will be against the SDGs and EU Green Deal [6].

To feed an expected global population of 9 billion in 2050, the Food and Agriculture Organization (FAO) estimates that the food production will need to increase by 70% [7]. In the agricultural sector, greenhouse technology, also known as closed agriculture, is strategic to rise the production and to help covering the worldwide demand since it provides a suitable microclimate for plants, thus facilitating optimal plant growth, extension of production duration, induction of earliness, and obtaining higher and better quality yields [8]. The global area of greenhouse's crops has been increasing during last years and is currently larger than 3 600 000 ha worldwide [9]. The two main regions of greenhouses in the world are located in eastern Asia, mainly in China [10] with estimations that go from 2 000 000 ha [11] to 3 346 800 ha [9], and in the Mediterranean countries. From those, Spain is the leading country, with 74 918 ha [12] of greenhouse agriculture, followed by Italy, with more than 62 000 ha [13], and Turkey with over 41 384 ha [14]. In the USA, the closed agriculture is not so important. The main region of greenhouses is California with just 210 ha [15]. Most of the greenhouse's vegetables consumed in the USA are imported from Mexico, which has a global area of closed agriculture of 40 000 ha [16]. However, although greenhouse technology is key to achieve long term food security, the thermal regulation of greenhouses requires higher energy demand resulting in a much higher greenhouse gas emissions [17,18]. Taking this into account, if renewable energy resources could be actively used in greenhouses, they could decrease the consumption of fossil fuels and grid electricity to further mitigate the GHGe from the agricultural sector [19–24].

Agriculture photovoltaics (AgriPV, APV, agrivoltaics, agriphotovoltaic) is the combination of photovoltaic power generation and agricultural activities on the same land to alleviate land-use competition between energy and food production [25,26]. Furthermore, there are important synergies that could benefit both the PV and the agriculture sector. On the one hand, a global analysis has demonstrated that croplands are the most promising areas for PV due to their typical high solar resource, medium temperature and relative humidity [27]. The potential of this new concept to achieve the stated goals is huge, as it was estimated that the energy demand could be offset by solar production even if less than 1% of the croplands were converted to agrivoltaic [28] . On the other hand, APV systems can help reducing the greenhouse temperature [29,30], which can be beneficial to reduce the energy demand in the warmer months. In addition, it has also been proven that APV contributes to increase the water efficiency in semi-arid and arid regions due to evapotranspiration reduction [31,27].

Despite its potential, APV also presents relevant constraints that need to be considered. In this sense, different demonstrative projects and modelling techniques are being developed worldwide to investigate different PV technologies and system configurations [32]. Among the different concerns, the shading produced by the PV system could negatively affect the plant photosynthesis and decrease the harvestable products [33]. Among the different strategies to overcome this issue, new wavelength-selective PV technologies (e.g. organic polymer, dye-sensitized, perovskite, etc.)[26], the implementation of new tracking systems to optimize shading control [34,35], or the use of semi-transparent PV modules with active and high-transparent parts [36,37], are being investigated. Regardless the type of PV, the point still remains on how much shading is tolerable for optimal plant growing [13,38,39]. During the last decade, several experiments have faced this issue, but they are still limited to a few locations and/or a limited number of varieties of plants, such as the investigation of four crops (potato, winter wheats, celeriac and clover glass) at one location in Germany [40], one crop (corn) at one location in Japan [41], or rice for two locations also in Japan [42] Hence, further studies are still needed to assess the PV capacity that can be installed without compromise the crop productivity for each particular application. The development of dual models to estimate energy generation and crop production has been also addressed. However, most of them just predict the incident irradiance at plant level without paying enough attention to the crop growing [43], while others use existing crop models, which are only useful for a limited number of species, and do not accurately consider the effects of the photon flux variations on the plants [44]. Taking this into account, the modelling techniques need to be also improved to accurately evaluate the potential of the technology and to increase our understanding of the crop productivity as function of the TPV technology, type of crop or weather variables of the location under consideration.

Bearing the above in mind, we conduct a state-of-the-art global evaluation of the potential of APV systems in greenhouses based on the use of a novel modelling procedure introduced in this work. For that, we introduce a detailed dual APV model, whose main outputs are the PV energy and the crop photosynthetic rate over a specific period of time as a function of the APV transparency. The methodology here proposed is based on three novel sub-models specially adapted to APV applications able to accurately estimate the PV and crop performance, namely: a) a solar radiation model that considers both the broadband and spectral content of the irradiance, b) a PV model that considers the features (cell technology, transparency level, etc.) and main performance metrics (spectral, temperature, angular, etc.) and c) a crop model that considers the relationship between the photosynthetic rate and the effective photon flux (spectral + broadband) that falls on the crops, which has been experimentally measured from multiple crop species. This methodology is beyond the current modelling techniques and includes key features to improve the current efforts in this direction. For instance, the solar radiation sub-model also includes the prediction of the spectral irradiance, which is key considering that crops are also quantum converters. Regarding the PV sub-model, it introduces a flexible procedure that could be easily adapted to any type of PV technology as a function of the efficiency and spectral transmittance of the PV materials. With regards to the crop sub-model, the procedure considers both the intensity and spectral irradiance that falls on the plants, which is fundamental as they only response to a particular waveband. In addition, this sub-model opens the way to further novel studies concerning the spectral performance of APV systems under the time-varying atmospheric conditions considering both the spectral properties of the PV technology and crop under consideration. To extend our results, we have further analysed four representative locations with a high potential of APV implementation because their atmospheric conditions and greenhouse concentration. These are El Ejido (Spain), Pachino (Italy), Antalya (Turkey) and Vicente Guerrero (Mexico). As a first step, we have considered semi-transparent c-Si technology due to its superior efficiency compared to any other transparent emerging PV technology, see Fig. 1. Also, this technology presents other relevant benefits such as its high stability, well-known outdoors performance and commercial availability. Regarding the crops, we focus on annual horticultural crops. In this sense, we measured the photosynthesis rates of 15 economically important species and experimentally characterized for their accurate modelling under the time varying solar irradiance. In addition, the coefficients of the crops experimentally investigated are also provided. So, they can be used by other researchers in future work.

Based on the detailed methodology introduced, the PV transparency

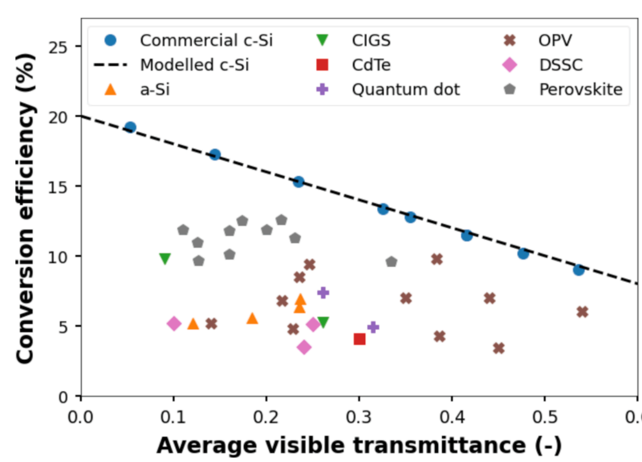

Fig. 1. Conversion efficiency as a function of the average visible transmittance of different PV technology taken from [45]. The efficiency of commercial c-Si technology from BISOL Group, d.o.o. has been also included (Bisol Lumina series: https://www.bisol.com/pv-modules). The modelling efficiency as a function of transparency of c-Si technology using the methodology proposed in this work is also shown for validation purposes.

levels investigated, and the number of crops and locations considered, this work could be considered as the first global study that could be found in the literature concerning the energy yield of APV systems for closed agriculture applications. The present investigation provides novel insights of the potential and performance of APV technology in greenhouses at global scale under a wide number of conditions (e.g. different atmospheric characteristics, PV transparencies or crops). Taking the above in mind, the results of this work are valid to offer fast and reliable solutions for increasing the competitiveness and energy efficiency of APV systems for greenhouses applications.

2. Methods and materials

We have developed a novel methodology to evaluate semi-transparent PV technology integrated on greenhouses, see Fig. 2. Thus, the global model is characterised by two main branches, one corresponding to the PV generator and the other to the crops. At the same time, the inputs are the PV technology specifications (e.g. cell technology or transparency), the atmospheric conditions of the location under study (e.g. irradiance or temperature), and the natural features of the crops selected (e.g. response to incident photon flux). This way, the model is general and can be adapted to any crop, location and, to the main semi-transparent PV technologies. The main output of the PV model is the energy harvested over a time interval in kWh/m^2, while the main output of the crop model is the CO_2 absorbed by photosynthesis during a time interval measured in mol(CO_2)/m^2. This methodology allows to investigate and optimize the relation between the PV energy harvested and the productivity of the crop. The features of the sub-models, as well as the input and output variables, are described in the next sub-sections. In addition, the main inputs and outputs of each sub-model are provided in Table 1.

2.1. Inputs description

2.1.1. PV module and transparency factor

In the proposed method, general semi-transparent PV modules could be considered. The modules can be made up of a transparent and a PV active area, see Fig. 3 (left). Based on this configuration, we define the PV module by a photovoltaic active factor (PVF), which represents the ratio of the solar cell area to the total module area as:

$$PVF = \frac{A_{active}}{A_{total}} \tag{1}$$

In this sense, the transparency of the PV module can be achieved by the combination of a highly transparent area (typically glass, with $\tau_{glass}(\lambda)$ transmittance) and an active PV area (solar cells with $\tau_{active}(\lambda)$ transmittance). Bearing this in mind, we propose a metric to quantify the

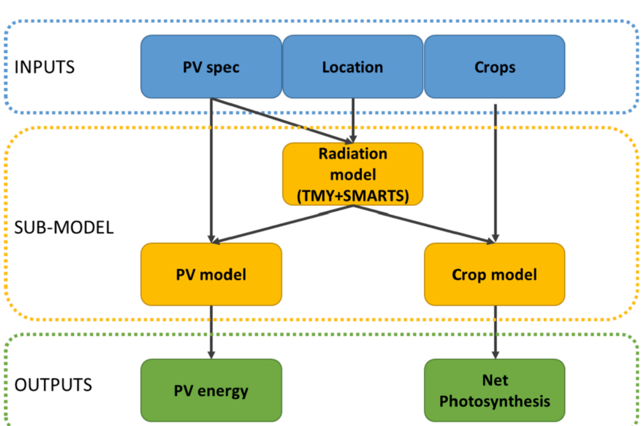

Fig. 2. Flow chart of the model of semi-transparent PV integrated on greenhouses.

Table 1
List of the main inputs and outputs of each sub-model.

Submodel	Inputs (units)	Outputs (units)
Radiation	Latitud (°) Longitud (°) Inclination (°) Orientation (°)	Global tilted irradiance (W/m^2) Direct tilted irradiance (W/m^2) Diffuse tilted irradiance (W/m^2) Spectral global tilted irradiance (W/m^2 nm)
	Typical meteorological year (GHI and DiffHI, W/m^2)	Spectral direct horizontal irradiance (W/m^2 nm) Spectral diffuse horizontal irradiance (W/m^2 nm)
PV	Global tilted irradiance (W/m^2) Spectral global tilted irradiance (W/m^2 nm) Module efficiency under STC (-) Photovoltaic Active Factor (-) Angle of Incidence (°) Spectral Response (A/W nm) Typical meteorological year (air temperature, °C)	Power per area (W/m^2) Energy per area (kWh/m^2)
Crop	Spectral direct horizontal irradiance (W/m^2 nm) Spectral diffuse horizontal irradiance (W/m^2 nm) Transparency factor (-) Angle of Incidence (°) Quantum yield of plants (-) Photosynthetic light-response curve (μmol CO^2/m^{2}s)	Net photosynthesis rate (mol CO^2/m^2)

global transparency of the PV module (TRF) by means of the following expression:

$$TRF(\lambda) = \left[\tau_{glass}(\lambda)\bullet(1-\mathrm{PVF}) + \tau_{\mathrm{active}}(\lambda)\bullet\mathrm{PVF}\right] \tag{2}$$

Based on this magnitude, it is also possible to define the transparency properties of the module for a specific wavelength as:

$$averageTRF = \frac{\int_{\lambda_{min}}^{\lambda_{max}} TRF(\lambda)d\lambda}{(\lambda_{max}-\lambda_{min})} \tag{3}$$

where λ_{max} and λ_{min} are, respectively, the maximum and minimum wavelength of the band considered. To the knowledge of the authors, there is no a standard definition of the wavelength limits to define the transparency of a PV module for APV applications. A possible range could be 400–700 nm since it is widely considered that the photosynthesis occurs within that region [46].

As mentioned above, we focus here on silicon-based semi-transparent modules because of the reasons outlined in the introduction section. This way, the $\tau_{active}(\lambda)$ has been set equal to 0, as c-Si solar cells are opaque. Fig. 3 (right) shows the typical quantum efficiency (EQE) of a c-Si solar cell together with the standard AM1.5 global spectrum. With regard to the $\tau_{glass}(\lambda)$, it has been estimated through a standard physical model of the cover glass of PV modules based on Snell's and Bougher's laws, as commented in [47]. As recommended in that study, a glazing coefficient of 4 m^{-1} and a refraction index of 1.526 have been used. The thickness has been set equal to 5 mm, which is approximately twice the recommended value for standard single-glass modules, as semi-transparent c-Si modules are expected to consist of a sandwich structure with a glass on the top and back of the solar cells [45]. Despite of this, it is also important to remark that the methodology introduced in this work could be easily adapted to study other module configurations and cell technologies in the future by including the specific geometry and materials properties, e.g. spectral transmittance of the cells.

2.1.2. Crops under study and experimental characterisation

Selected plant species for this study are given in Table 2 and were chosen according to three non-exclusive criteria. First, those species that are economically important and grown in a significant extent under

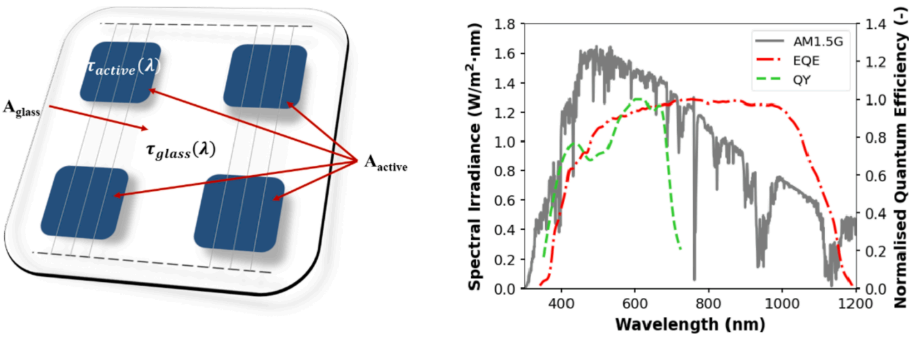

Fig. 3. Left: scheme of a semi-transparent PV module composed of a transparent and a PV active area. Right: standard ASTM G173-03 global spectrum (U.S Standard Atmosphere 1976, S&F rural aerosol model, aerosol optical depth at 500 nm = 0.084 and water vapour = 1.42 cm) [48], typical quantum yield (QY) of the crops [49] (with an absorption band between 400 and 700 nm approximately) and external quantum efficiency (EQE) of c-Si [50] (with an absorption band between 400 and 1100 nm approximately).

Table 2
Plant species included in study. For each crop, the harvested area in the study regions is shown. For each taxon, the maximum photosynthetic rate (A_{max}) and the optimal photosynthetic photon flux density (PPFD) are also given.

Family	Species (common name)	Area (ha)*	A_{max} (μmol·CO_2/m^2s)	Optimal PPFD (μmol/m^2s)
Cucurbitaceae	*Citrullus lanatus* Schrad. (Watermelon)	1,625,088	12.0	900
	Cucumis melo L. *(Santa Claus melon)*	1,778,962	6.14	850
	Cucumis melo L. *var. Inodorus (Canary melon)*	–	6.62	800
	Cucurbita pepo L. *(Zucchini)*	644,793	8.52	850
	Cucumis sativus L. (Cucumber)	1,320,447	11.76	850
Fabaceae	*Arachis hypogaea* L. (Peanut)	4,589,750	13.92	1150
	Pisum sativum L. *(Pea)*	1,722,962	9.35	750
Solanacae	*Capsicum annuum* L. (Pepper)	1,069,756	9.83	800
	Solanum melongena L. (Eggplant)	820,385	8.29	800
	Solanum lycopersicum Lam. *var.* “Berner Rose” (Berner Rose tomato)	1,500,208	10.2	800
	Solanum lycopersicum Lam. *var.* (Green Zebra tomato)	–	9.21	750
Poaceae	*Brachypodium distachyon* L. (Purple false brome)	n.a.	13.38	1150
	Brachypodium stacei C. (False brome)	n.a.	16.4	1000
Rosaceae	*Fragaria vesca* L. (Strawberry)	170,645	10.92	850
	Rubus ideaeus L. (Raspberry)	9878	12.02	850

* Source: 2019 FAOstat (http://www.fao.org/faostat/es/#data/QC).

closed cultivation conditions in the geographical areas analysed. Second, plant species which photosynthesis only uses the Calvin cycle for fixing CO_2 catalysed by ribulose-1,5-bisphosphate carboxylase (Rubisco), namely C3 plants [51]. Third, dicots and monocots are represented. Regarding this last criterion, we included two diploid monocots species *Brachypodium distachyon* and *B. stacei*, which are important species for temperate cereals worldwide [52]. Thus, we analysed a total of 15 taxa (15 species and 5 varieties, see Table 2) for gas exchange measurements in relation to light intensity.

Seeds from these species were supplied by Rocalba® Co. and were placed into Petri dishes at 4 °C during 7 days for cold stratification. Once germinated, they were individually planted and grown on a mix of perlite and standard soil (0.5:1 v/v) in 7x7x10 cm^3 pots. Plants were grown under controlled conditions in a growth chamber (22 °C; 16 h white light/ 8 h dark, 600 μmol $m^{-2}s^{-1}$; relative humidity: 60%). After 3–4 weeks of growth, once plants developed the first pair of true leaves, we measured photosynthetic light-response curves on fully-expanded leaves for each species (three biological replicates per species) using an infrared gas analyser (Licor LI-6800 portable photosynthetic system). Leaves were acclimated to a photosynthetic photon flux density (PPFD) of 3000 μmol/m^2·s (R90, B10 light) for the first measurement, and subsequent measurements were made by decreasing PPFD at 200 μmol/m^2·s intervals to 50 and 0 μmol/m^2·s. At each interval, photosynthesis stabilization was attained after 2 min. Cuvette air temperature was 22 °C, and cuvette CO_2 concentration 399 ± 0.1 μmol/mol during measurements. Fig. 4 shows an example of the photosynthetic light-response curve and growing crop for the case of the Green Zebra Tomato.

2.1.3. Locations under study

As commented, it has been already demonstrated that the synergies achieved through the combination of agriculture and photovoltaics can be maximized in arid regions [27,31]. In addition, most of the relevant areas for greenhouse cultivation are located on East Asia, around the Mediterranean Sea and in North-West America. In this work, we have selected four locations for our dual APV model, see Table 3, according to two criteria. The first one is the density of greenhouses in the region, while the second is related to the climatic condition. In particular, we have only considered locations with arid or semi-arid and temperate climate, according to Köppen-Geiger (K-G) climate classification, which is the most widely used climate classification, based on a large global data set of long-term monthly precipitation and temperature station time series worldwide [53]. For these locations, the solar radiation and meteorological data, e.g. temperature and humidity, have been obtained from PVGIS database. Based on these criteria, therefore, it could be stated that the conclusions of this work are representative of locations with a high penetration of greenhouses and with favourable conditions for the implementation of PV technology.

2.2. Sub-models description

2.2.1. Solar radiation model

The outputs of the solar radiation model are both broadband irradiances (global tilted irradiance, *G*, direct tilted irradiance, *D*, and diffuse tilted irradiance, *Diff*, all of them taking the plane of the PV array as reference) and spectral irradiances (global tilted spectral irradiance, $E_G(\lambda)$, direct horizontal spectral irradiance, $E_{DH}(\lambda)$, and diffuse horizontal spectral irradiance, $E_{DiffH}(\lambda)$). To get these outputs, the model combines information from the Typical Meteorological Year (TMY) from PVGIS database, which includes hourly values of global and diffuse horizontal irradiances (*GHI* and *DiffHI*) over one typical year for the analysed location, and from the Simple Model of the Atmospheric

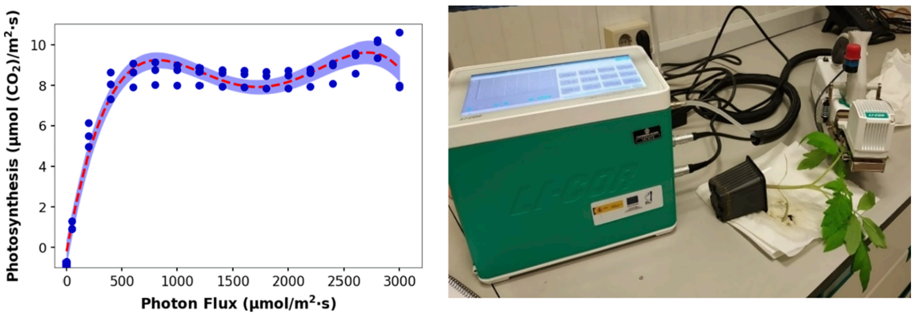

Fig. 4. Left: Photosynthesis vs photon flux for the Green Zebra Tomato. Right: Licor 6800 Infrared Gas analyser and growing crop. (For interpretation of the references to colour in this figure legend, the reader is referred to the web version of this article.)

Table 3
Selected location with annual solar radiation, meteorological relevant information, total greenhouse area and average area per greenhouse.

City (country)	Geog. coordinates (latitude, longitude)	G-K climatic condition	Tot. irradiation (kWh/m^2)	Avg. T_{air} (°C)	Avg. H_r (%)	Tot. greenhouse area (ha)	Avg. greenhouse area (m^2)
El Ejido (Spain)	36.7, −2.8	BWk	1925.21	18.92	60.28	4586*	10,500 [54]
Vicente Guerrero (Mexico)	30.7, −116.0	BSh	2098.971	16.43	80.52	4400**	23,500**
Pachino (Italy)	36.7, 15.0	Csa	1838.33	19.1	77	7300***	16,000 [55]
Antalya (Turkey)	36.9, 30.71	Csa	1852.82	20.25	63.6	10,963 [56]	48,000 [56]

* Ministerio de Agricultura, Pesca y Alimentación. Gobierno de España: https://www.mapa.gob.es/es/estadistica/temas/estadisticas-agrarias/agricultura/superficies-producciones-anuales-cultivos/.
** Gobierno de México. http://infosiap.siap.gob.mx/gobmx/datosAbiertos.php.
*** Istat Statistics. http://dati.istat.it/?lang=en#.

Radiative Transfer of Sunshine (SMARTS) [57] , which allows spectral irradiances under clear sky conditions to be generated. SMARTS is able to compute the distribution of solar power or photon energy for each wavelength of light reaching the Earth's surface, and has been extensively validated and used in several fields such us solar energy, architecture, atmospheric science, photobiology, or health physics over the last 25 years [58].

TMY data is used to estimate the hourly values of D, Diff and, G. In this work, D is proposed to be obtained by a trigonometric conversion, see Fig. 5, of the direct horizontal irradiance (whose value is GHI – DiffHI) considering the angle-of-incidence (AOI) of the solar beams with respect to the normal of the PV field and the sun's zenith angle (Z) as:

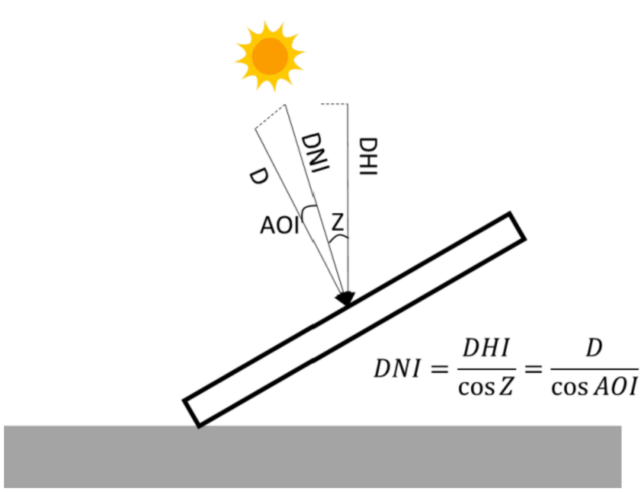

Fig. 5. Scheme to explain the formulation of equation (4). Note that the DHI is the projection of the DNI on the vertical axis according to the Z angle, and the D is the projection of the DNI on the perpendicular axis of the module surface according to the AOI.

$$D = (GHI - DiffHI)\bullet\frac{\cos AOI}{\cos Z} \quad (4)$$

Diff can be broken down into two components, sky diffuse and ground reflected, which are estimated by isotropic models as:

$$Diff = \frac{1+\cos\beta}{2}\bullet \mathrm{DiffHI} + \frac{1-\cos\beta}{2}\bullet\rho\bullet \mathrm{GHI} \quad (5)$$

The sky diffuse component corresponds to the first adding and the ground reflected component corresponds to the second adding. In this expression, β is the tilt angle of the PV generator and ρ is the albedo coefficient. In the current study, equator-pointed with tilt equal to latitude PV modules are considered and ρ is set to 0.2 as an average value of

albedo. *G* is calculated simply as the sum of *D* and *Diff*.

The SMARTS software is used to generate the global tilted, direct horizontal, and diffuse horizontal spectral irradiances under clear sky conditions. These spectra are scaled to match the *G*, *DHI* and *DiffHI* broadband irradiances obtained from TMY as a way to account for the clouds and avoiding the overestimation of the total solar budget as:

$$E_I(\lambda) = \frac{I}{\int E_{I,SMARTS}(\lambda)\bullet d\lambda}\bullet \mathrm{E}_{\mathrm{I,SMARTS}}(\lambda) \quad (6)$$

where the term *I* refers to the component of the irradiance to be scaled.

2.2.2. Photovoltaic model

The PV harvested power per unit generator area (*P*/*A*) is calculated following a standard procedure based on the next expression [59,60]:

$$P/A = G\bullet\eta_{\mathrm{TPV,STC}}\bullet\mathrm{AOIF}\bullet\mathrm{SF}\bullet\mathrm{TF} \quad (7)$$

where $\eta_{TPV,STC}$ represents the transparent PV module efficiency under Standard Test Conditions (STC) (1000 W/m^2, AM1.5G spectrum and 25 °C), *AOIF* is the angle-of-incidence factor that corrects the PV power when the sunrays do not fall perpendicularly on the module surface, *SF* is the spectral factor that spectrally corrects the PV power and, *TF* is the thermal factor that performs the temperature correction. The four factors are dimensionless and expressed in per unit.

The $\eta_{TPV,STC}$ is obtained from the module efficiency under STC, $\eta_{mod,STC}$, as:

$$\eta_{TPV,STC} = \eta_{cell,STC} \bullet \mathrm{PVF}\hat{\mathrm{A}}\cdot(1 - \mathrm{L_{mod}}) = \eta_{\mathrm{mod,STC}} \bullet \mathrm{PVF} \tag{8}$$

where $\eta_{mod,STC}$ is going to depend on the efficiency of the cells, $\eta_{cell,STC}$, and on the potential internal losses of the PV module (L_{mod}), such as wiring and mismatch losses. In this study, $\eta_{mod,STC}$ has been set to 0.20 as a typical value for commercial crystalline silicon technology. For validation purposes, Fig. 1 shows the modelled and experimental efficiency of a commercial c-Si TPV module. As can be seen, the efficiency is predicted with an almost perfect fit, a determination coefficient (R^2) of 0.99.

The *AOIF* is calculated as:

$$AOIF = \frac{D \bullet F(AOI) + Diff}{G} \tag{9}$$

where *AOI* is the angle-of-incidence of the solar beams with reference to the normal of the PV module and *F(AOI)* is the angle-of-incidence modifier function. This equation assumes that the diffuse irradiance is isotropic in a first approximation. Hence, only the direct irradiance has been corrected in angle. The angular correction function has been estimated by means of the Snell's and Bougher's laws and the properties of the module previously discussed in sub-section 2.1.1., see also [47] for further details.

The *SF* is calculated as [61]:

$$\frac{SF = \int E_G(\lambda) \bullet SR(\lambda) \bullet d\lambda}{\int E_{G,ref}(\lambda) \bullet SR(\lambda) \bullet \mathrm{d}\lambda \bullet \frac{\mathrm{G_{STC}}}{\mathrm{G}}} \tag{10}$$

Where $SR(\lambda)$ is the spectral response of the solar cell material, see Fig. 3 (right), $E_{G,ref}(\lambda)$ is the standard ASTM G173-03 global spectrum [48], and G_{STC} is the STC global irradiance of 1000 W/m^2. The integrals in the equation above comprise the whole spectral range and are limited by the waveband of the PV material under investigation.

The *TF* is calculated from the temperature coefficient of efficiency of the PV material, γ, as:

$$TF = 1 + \gamma \bullet \left(\mathrm{T_{cell}} - \mathrm{T_{cell,STC}}\right) \tag{11}$$

where T_{cell} is the cell temperature and $T_{cell,STC}$ is the cell temperature under STC ($T_{cell,STC} = 25\ °C$). The T_{cell} is estimated from the ambient temperature, obtained from the TMY, and the global tilted irradiance following the method described in the IEC 61853–1 standard and based on the Nominal Operating Cell Temperature (*NOCT*). In this study, the *NOCT* has been set equal to 45 °C and the γ equal to −0.0039 1/°C as representative of c-Si modules.

The *P/A* obtained with the expressions above can be integrated over the time interval of interest to get the PV harvested energy in kWh/m^2, which is the main output of the PV model.

The methodology to predict the solar resource and the PV energy output proposed above is mainly based on a novel combination of procedures and tools available in the literature. In addition to this, for validation purposes, Fig. 6 shows the modelled and recorded average annual and monthly daily PV energy for a standard c-Si PV module (PVF = 1) located at the rooftop of the CEACTEMA research centre of the University of Jaén. The modelled values have been obtained using the solar radiation and PV sub-models previously described. As can be seen, the methodology shows a high accuracy with an annual Mean Absolute Relative Error around 2%. This, together with the accuracy to predict the efficiency of TPV modules with transparency commented above, provides further assurance of the procedure used to predict the output of APV technology at the selected locations.

2.2.3. Crop model

In this work, we introduce a method to evaluate the crops productivity by considering the incident spectral irradiance and the spectral absorption of the plants. Based on the commented in the previous subsections, the spectral irradiance incident on the plants can be obtained from the direct and diffuse horizontal solar spectra and the spectral transmittance of the glass, $\tau_{glass}(\lambda)$, and the PV active area, $\tau_{active}(\lambda)$. At this stage, it is assumed that the PV cover is mounted at enough height from the ground, so that the light is considered homogenously distributed when falling on the plants, i.e. the discontinuities (shaded area/unshaded area) are filtered. Taking the above into account, the weighted average spectrum incident on the plants, $E_{plant}(\lambda)$, is proposed in this work to be computed as:

$$E_{plant}(\lambda) = \left[E_{DH}(\lambda) \bullet \mathrm{F(AOI)} + \mathrm{E_{DiffH}}(\lambda)\right] \bullet \mathrm{TRF}(\lambda) \tag{12}$$

From this spectrum, in W/(m^2•nm), it necessary to estimate the PPFD, in µmol/(m^2•s), in order to predict the photosynthetic rate of each particular crop according to the experimental measurements described in sub-section 2.1.2. This can be performed according to the next expression [46]:

$$PPFD_{plant} = \int_{400}^{700} \frac{E_{plant}(\lambda)\hat{\mathrm{A}}\cdot\lambda}{N_A \bullet h \bullet c} \bullet \mathrm{d}\lambda \tag{13}$$

where N_A is the Avogadro's number, h is the Planck's constant and c is the light speed.

In addition, the light source of the Licor LI-6800 unit used to char-

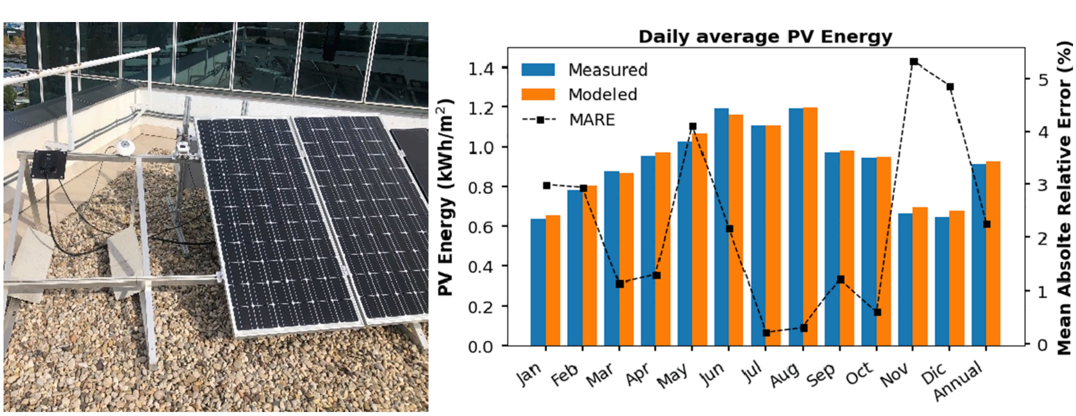

Fig. 6. Set-up and experimental validation of the methodology to predict the energy output (monthly and annual daily average) of PV technology conducted at CEACTEMA of the University of Jaén. See refs. [62,63] for further details of the experimental set-up.

acterise the different crops has a spectral distribution, $E_{Licor}(\lambda)$, that differs from the actual incident spectrum on the plants. In particular, this light source is composed of two LEDs (a blue LED with peak spectral irradiance at 456 nm and a red LED with peak spectral irradiance at 662 nm). Hence, in order to improve the accuracy of the results, a spectral correction or mismatch spectral factor (*MM*) must be also considered. This *MM* correction factor, which is introduced in this work, can be obtained by means of the following expression:

$$MM = \frac{\int E_{plant}(\lambda)\hat{A}\cdot QY(\lambda)\hat{A}\cdot\lambda\bullet d\lambda}{\int E_{Licor}(\lambda)\hat{A}\cdot QY(\lambda)\hat{A}\cdot\lambda\bullet d\lambda}\bullet\frac{\int \mathrm{E}_{\mathrm{Licor}}(\lambda)\hat{A}\cdot\lambda\bullet \mathrm{d}\lambda}{\int \mathrm{E}_{\mathrm{plant}}(\lambda)\hat{A}\cdot\lambda\bullet \mathrm{d}\lambda} \tag{14}$$

where $QY(\lambda)$ is the spectral quantum absorption of the crop or quantum yield. In this case, we have used the typical crop spectral absorption function proposed by McCree [49], see Fig. 3 (right), which is still widely considered as representative of crops [46]. It is also important to highlight the MM factor above, in combination with equation (12), opens the way for novel studies concerning the spectral performance of APV systems, considering both the spectral transmittance of PV technology and the quantum absorption of plants, such as those widely conducted for the investigation of PVs in outdoors [61]. The $E_{Licor}(\lambda)$ has been obtained from the technical documentation of the equipment. Due to this relationship, the obtained $PPFD_{plant}$ can be accurately related to the PPFD emitted by the Licor according to the next expression:

$$PPFD = MM\hat{A}\cdot PPFD_{plant} \tag{15}$$

The relation between the PPFD and the photosynthetic rate (PSN) in $\mu mol(CO_2)/(m^2\cdot s)$ is a characteristic function specific for each crop. This relationship has been experimentally found for each specie following the procedure described in section 2.3, and fitted to a fourth-order polynomial:

$$PSN = a_0 + a_1\hat{A}\cdot PPFD + a_2\hat{A}\cdot PPFD^2 + a_3\hat{A}\cdot PPFD^3 + a_4\hat{A}\cdot PPFD^4 \tag{16}$$

The polynomial coefficients obtained for each crop analysed are listed in the Annex. As can be seen in this annex, the PSN is modelled with a high accuracy, an average R^2 of 0.90 has been found. This provides further assurance of the quality of the modelling of the crops under investigation. The instantaneous PSN can be finally integrated over the time interval of interest to get the CO_2 produced by the photosynthesis in mol $(CO_2)/m^2$, which is the main output of the crop model.

3. Results

The first step to investigate the potential of APV systems for greenhouses is to select the optimum balance between the PV yield and crop productivity. The shading caused by the PV system reduces the photon flux that falls on the crops. As a consequence, it tends to reduce the photosynthesis. In this study, we define the optimum PV system as the one that reduces the annual PSN by only 10%. Under this scenario, it could be considered that the PV system does not play an important role in the crop growing, or at least it has a marginal impact. For doing this, we vary the TRF from 0 (fully opaque PV system) to 1 (fully transparent PV system) for each crop and location under evaluation. Fig. 7 shows an example of the optimization procedure for the Green Zebra Tomato for the four locations. As can be seen, the increase of the TRF reduces the PV harvested and increases the crop performance. For this case, the optimum TRF is similar and presents a minimum of 0.57 (Vicente Guerrero) and a maximum of 0.62 (Pachino). Under this scenario, the PV energy harvested ranges from 155.8 (Pachino) to 199.0 (Vicente Guerrero) kWh/m^2, while the annual PSN ranges from 98.0 (Antalya) to 99.8 (Pachino) $mol(CO_2)/m^2$.

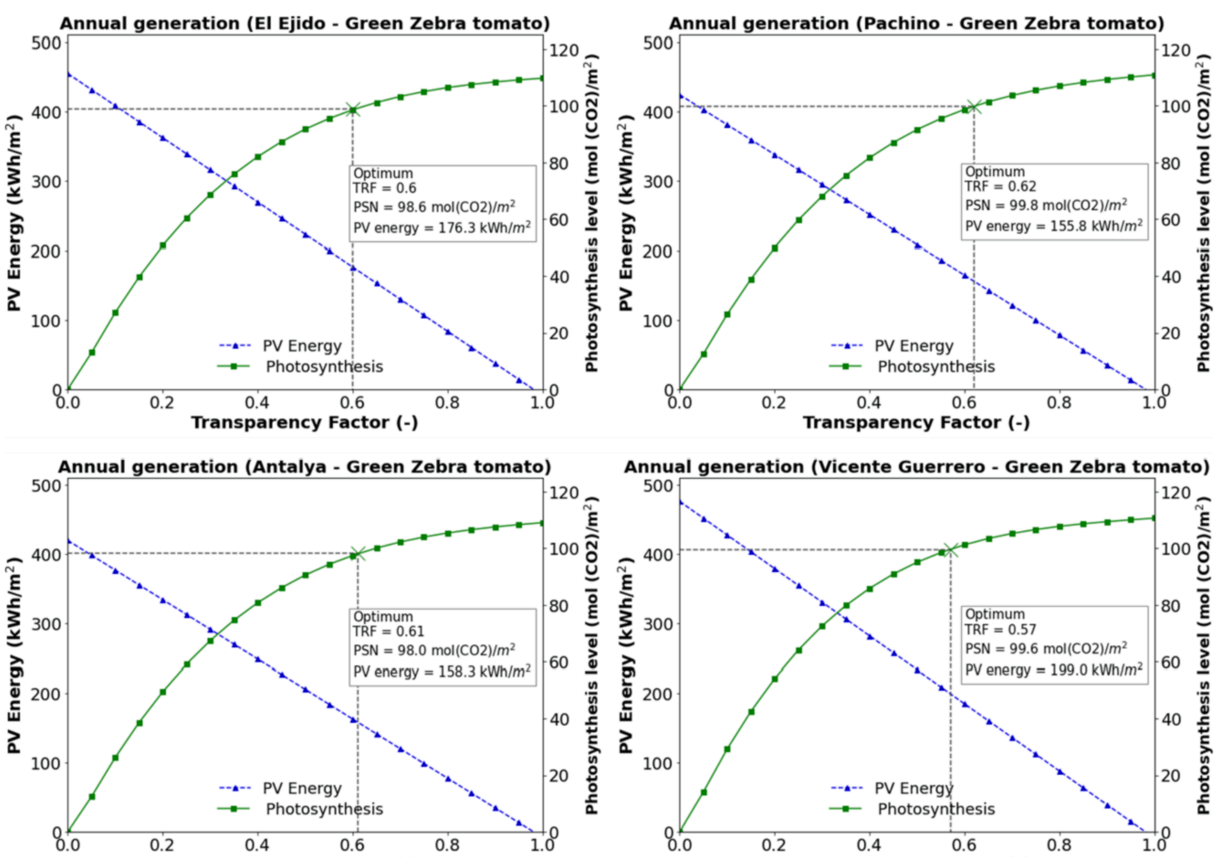

Fig. 7. Relationship between the PV energy and PSN as a function of the transparency of the modules for the Green Zebra Tomato for the four selected locations. (For interpretation of the references to colour in this figure legend, the reader is referred to the web version of this article.)

Fig. 8 shows the results for all the crops and locations under study. For a better analysis, the species are also grouped in families. The TRF values obtained are presented in Fig. 8 (top). Overall, it could be stated that the higher the annual solar resource the lower the transparency of the modules. This can be clearly seen for the case of Vicente Guerrero, see Table 3 for the irradiation data, which systematically presents the lowest TRFs for all the species with values ranging from 0.57 to 0.74. In addition, El Ejido, which has the second annual irradiation, shows the second lowest TRFs in the majority of the cases with values ranging from 0.60 to 0.80. Finally, Pachino and Atalya, with almost equal annual irradiations, show a similar TRF for all the cases with values ranging from 0.67 to 0.77. It is also worth mentioning that the type of crop has a remarkable impact on the TRF, and therefore in the PV capacity. This phenomenon can be explained considering the photon flux at which the different crops reach their maximum photosynthetic rate, see Table 2. For instance, the lowest TRFs are achieved for the Green Zebra Tomato and the Pea, which has the minimum optimal PPFD of 750 μmol/m^{2}s, with values ranging from 0.57 (Vicente Guerrero) to 0.62 (Pachino). On the other hand, the Peanut presents the highest TRFs with values ranging from 0.74 (Vicente Guerrero) to 0.80 (El Ejido), which has the maximum optimal PPFD of 1150 μmol/m^{2}s. This is an important finding as the PV capacity is going to depend on the level of the optimal PPFD. In other words, the lower the PPFD at which the A_{max} is achieved the lower the TRF, and therefore, the higher the capacity of the PV system without significantly affecting the crops performance. Overall, it can be stated that the Solanacae family allows lower TRF to be achieved due to their lower optimal PPFD, while the Poaceae tends to produce the highest TRF values due to their higher optimal PPFD.

Fig. 8 (middle) shows the annual PSN for all the species investigated for the locations under study. As can be seen, the crop productivity is similar at each site, although it tends to be slightly higher in Vicente Guerrero due to its higher solar resource. As commented, these values are found to be 10% lower than the total PSN that could be obtained in the absence of a PV system. In this sense, the PSN obtained at each site is mainly determined by the annual irradiation and the crop response to photon flux. The differences in the productivity of the crops shown in this figure can be explained considering the photosynthetic rate of each specie. In particular, it could be affirmed that the higher the A_{max} the higher the PSN. For instance, the maximum PSN is obtained for the False brome, which has the maximum A_{max} of 16.4 μmol(CO_2)/m^{2}s, with values ranging from 173.1 (Antalya) to 178.7 (Vicente Guerrero) mol (CO_2)/m^2. On the contrary, the minimum is obtained for the Santa Claus Melon, which has the minimum A_{max} of 6.14 μmol(CO_2)/m^{2}s, with PSN values ranging from 64.7 (Antalya) to 67.5 (Vicente Guerrero) mol (CO_2)/m^2. It is important to mention that the selection of the most suitable crops is going to depend on many other factors than in a purely analysis through the PSN parameter, e.g. commercialization potential. This means that the crops with the higher PSN shown in the figure are not going to be necessarily the most interesting from an agricultural perspective. Despite of this, these values are expected to serve as reference for other work focused on the investigation of other species and families, PV technologies, locations or based on different optimization criteria.

The PV annual energy at each site is shown in Fig. 8 (bottom). As expected, the total energy is directly related to the TRF of the APV system and the annual irradiation. In this sense, Vicente Guerrero and El Ejido present the highest yields with values within 116.6–199.0 kWh/m^2 and 101.6–147.9 kWh/m^2, respectively. On the other hand, Pachino and Antalya have lower yields with values within 90.9–155.8 kWh/m^2 and 89.9–158.33, respectively. This way, the locations with high annual irradiations are benefit from two phenomena. On the one hand, they allow lower TRF values, and therefore a larger PV capacity, to be achieved while producing the same impact on the annual PSN. On the other hand, the larger PV capacity, in combination with the higher solar resource, allows more energy to be produced by the PV system. For instance, Vicente Guerrero has around 14% more irradiation than Pachino, but produces around 21%–32% more energy. This is a remarkable finding for selecting the most suitable locations and increasing the competitiveness of APV in greenhouses.

Another important result is the relation between the crops and the PV energy harvested. As commented above, the crops that are characterized by low optimal PPFD permits lower TRF values without significantly affect the crop productivity. Taking this into account, they will permit significantly higher energy yields than the crops characterized by a high optimal PPFD. For instance, the Green Zebra Tomato and the Pea show the maximum PV energy with values within 155–199 kWh/m^2. On the other hand, the Peanut shows the lowest energy yields with values ranging from 83.5 to 116.6 kWh/m^2. This means that the selection of the type of crop is also going to be crucial for maximizing the energy produced at each location, and therefore, for increasing the competitiveness of the whole APV system. Taking this into account, the Solanacae, followed by the Rosaceae and the Curcubitaceae, seems to be most suitable families for APV applications in greenhouses.

Fig. 9 summarizes the main results obtained for each location under study. In particular, it shows the transparency factor (top), and photosynthetic rate (middle), and annual PV energy harvested (bottom). As can be seen, the results are quite similar among the four locations. This can be explained considering that they have similar weather and irradiation conditions. Regarding to the annual optimal TRF, its mean value ranges from a minimum of 0.66 (Vicente Guerrero) to a maximum of 0.69 (Antalya and Pachino). The PSN shows even a more stable behaviour with annual mean values ranging from 111.0 (Antalya) to 113.9 (Vicente Guerrero) mol(CO_2)/m^2. On the other hand, the PV energy harvested shows the maximum variation among the three parameters. As stated above, this is consequence of the difference TRF and annual irradiation values at each location. In this sense, the annual mean PV energy harvested ranges from 124.05 (Pachino) to 156.3 (Vicente Guerrero) kWh/m^2.

Finally, Fig. 10 summarizes the model outputs (PSN and PV energy) and the optimal TRF and PVF considering the four locations under study. In this figure, the PVF parameter has been also included. It is true that in this study this parameter is mainly determined by the TRF due to the use of silicon-based semi-transparent modules. However, we have considered interesting to also include it to clearly state the PV active area. Based on these results, it could be concluded that it could be possible to develop APV systems with a TRF around 0.68 without significantly affecting the crop performance. This corresponds to an annual PVF of around 0.31 for the case of c-Si modules based on opaque solar cells. With regards to the crops, the results show that they have a global PSN around 112 mol (CO_2)/m^2. At the end, the results show that it would be possible to generate around 135 kWh/m^2 by using APV systems.

To illustrate the relevance of these results, Table 4 shows the total PV energy per region and per greenhouse for the areas listed in Table 3. In addition, the contribution of the APV system to the total market share of each country and the percentage of greenhouse self-consumption are also included. With regards to the greenhouse, a case of study based on an installation equipped with heating and cooling (GSHP), and lighting discussed in previous work [64], has been also considered. In this case, the energy is assumed to be only used for self-consumption, as it could be considered the most representative application of APV systems for greenhouse farming. As can be seen, the global implementation of APV systems in each region could contribute to the total energy share with values ranging from 2.3% at México to 6% at Turkey. With regards to the self-consumption, it would be possible to cover a minimum of 75% (México) in the worst case-scenario, and up to the whole energy demand in some favourable scenarios (Spain and Turkey).

4. Conclusions

This paper investigates the potential of agrivoltaics (APV) from greenhouses applications at global scale for the first time. For that, we have introduced a novel dual APV model that considers the key steps to

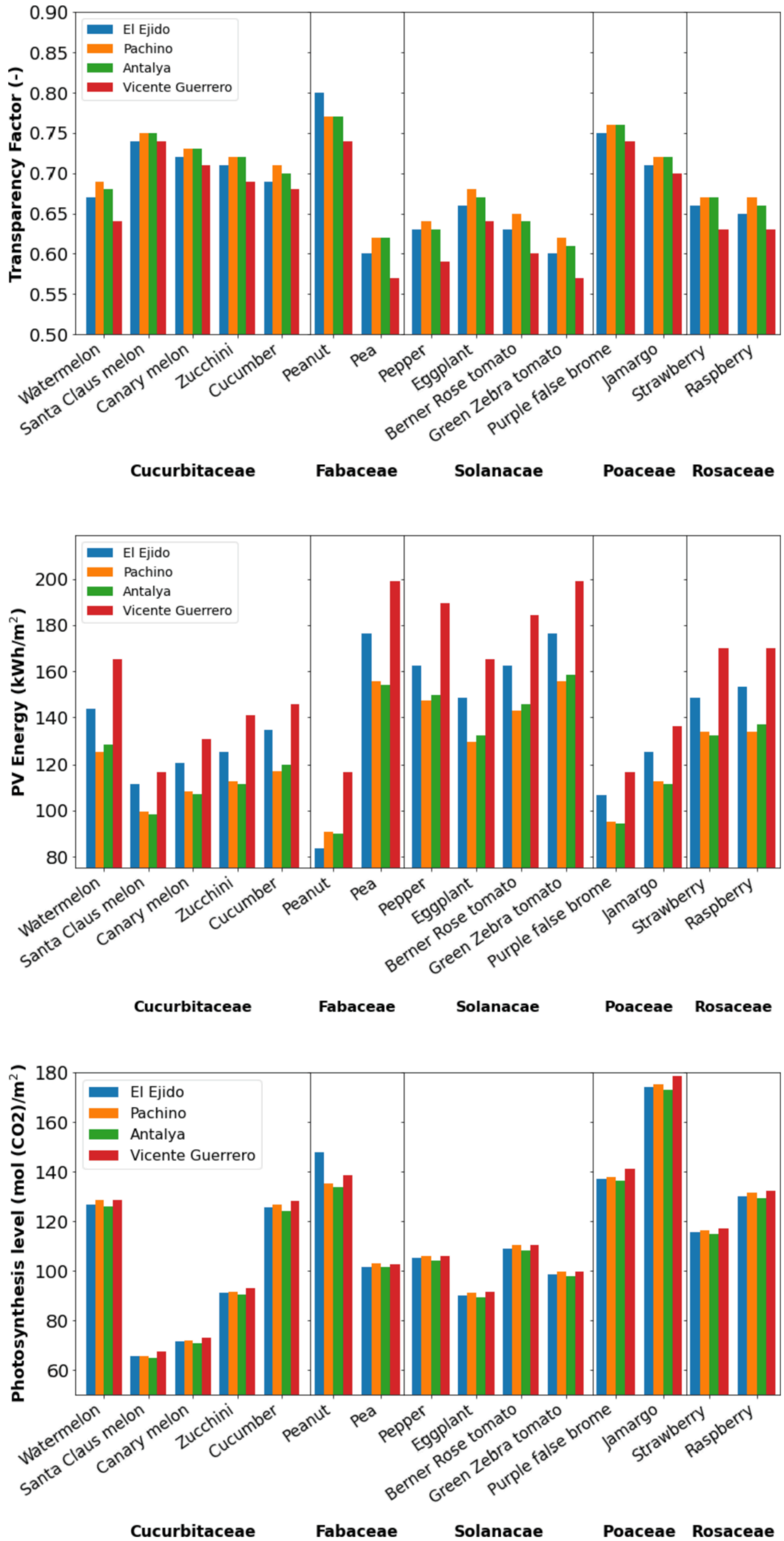

Fig. 8. Annual optimum TRF (top), PSN (middle) and PV energy (bottom) for each specie and family for the four locations under study.

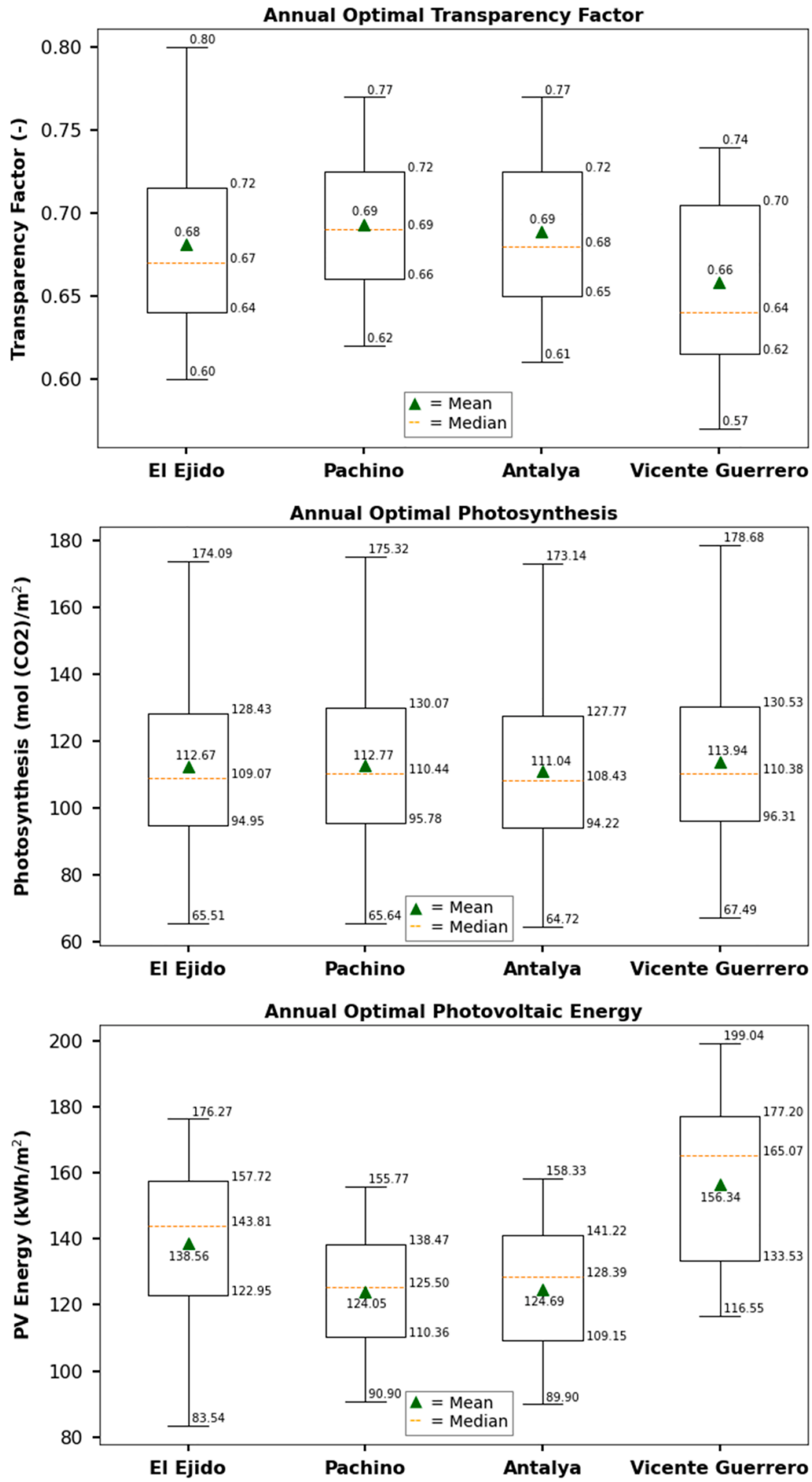

Fig. 9. Mean, median, maximum, minimum and percentiles 25 and 75 (represented by the boxplots) of the annual optimal transparency factor (TRF), photosynthetic rate (PSN), and PV energy harvested for each location.

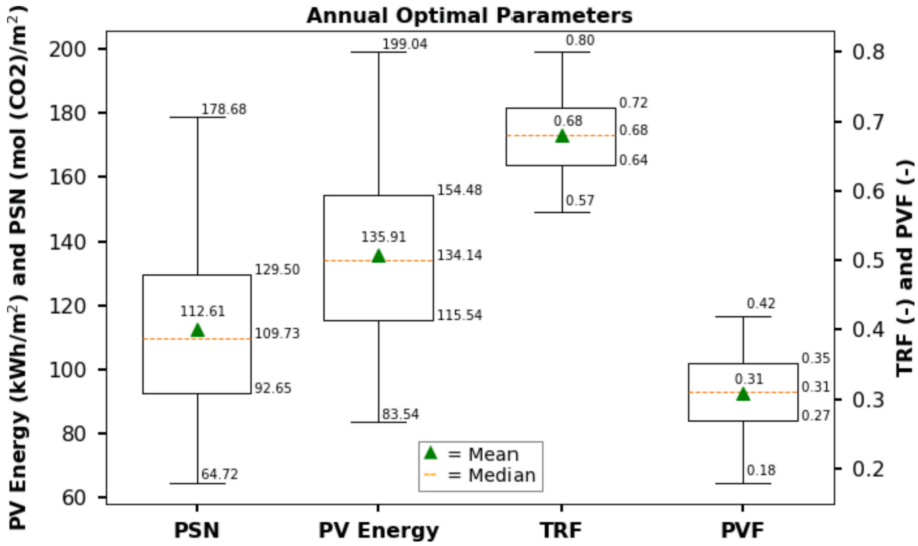

Fig. 10. Mean, median, maximum, minimum and percentiles 25 and 75 (represented by the boxplots) of the optimal transparency factor (TRF), photosynthetic rate (PSN), photovoltaic active factor (PVF) and PV energy harvested considering the four locations under study.

Table 4
PV energy harvested per region and resultant market share per country (data from total energy consumption per country are in GWh: 249 991 (Spain), 267 911 (México), 297 150 (Italy) and 251 367 (Turkey); source: https://datosmacro.expansion.com/energia-y-medio-ambiente/electricidad-consumo), and PV energy harvested and percentage of self-consumption per greenhouse assuming a consumption range of 137–165 kWh/m^2 (heating + cooling (GSHP) + lighting) [64].

City (country)	PV energy per region (GWh)	PV energy share (%)	PV energy per greenhouse (MWh)	Self-consumption per greenhouse (%)
El Ejido (Spain)	6354	2.5	1455	84–101
Vicente Guerrero (Mexico)	6096	2.3	3256	75–91
Pachino (Italy)	10,115	3.4	2217	76–91
Antalya (Turkey)	15,190	6.0	6651	95–114

accurately estimate the PV technology and crop performance beyond the current state-of-the-art modelling techniques. Accordingly, we have selected four representative locations with a high greenhouse implantation: El Ejido (Spain), Pachino (Italy), Antalya (Turkey) and Vicente Guerrero (Mexico). Concerning the PV technology, we have considered semi-transparent c-Si technology based on opaque cells due its high efficiency and reliability. Regarding the crops, 15 representative species from 5 different families, i.e. Cucurbitaceae, Fabaceae, Solanacae, Poaceae, Rosaceae, have been growth and experimentally investigated for their accurately evaluation under actual conditions. In this work, we have optimized the APV system by adjusting the transparency factor (TRF) of the modules to only reduce a 10% of the annual photosynthetic rate (PSN) of each specie, suggesting that, the PV system does not interfere with crop growing.

Findings of this work indicate that APV systems would have TRF values around 0.68. Moreover, the type of crop and annual irradiation at each site have a remarkable impact on the optimum TRF. In this sense, the lower the photon flux at which the crops reach their maximum photosynthetic rate the lower the TRF, and therefore, the larger the PV capacity. In addition, we have also found that the higher the solar resource the lower the TRF. Based on these two findings, it would be possible to achieve TRF values below 0.60 under some favourable scenarios. The results also indicate that the global crop productivity, evaluated through the PSN parameter, is around 112 mol (CO2)/m^2. The annual PSN at each site is mainly determined by the crop response to the incident photon flux. Finally, for the locations under study, we have found that the APV systems could produce an energy of around 135 kWh/m^2. As for the case of the TRF, the total energy yield is significantly affected by the type of crop selected. In this sense, the Solanacae, followed by the Rosaceae and the Curcubitaceae, seems to be most suitable families for achieving the highest energy yields. Under a favourable scenario, it would be possible to obtain energy yields close to 200 kWh/m^2. To contextualize these results, it is noticeable to mention that the average energy yield produced by APV systems would represent a contribution to the total energy market between 2.3% (México) and 6.0% (Turkey). In addition, it would be also possible to cover the whole consumption demand of a hypothetical greenhouse equipped with heating and cooling (GSHP), and lighting, under different favourable scenarios.

As previously commented, this work covers the study of 15 annual horticultural crops. In order to extend this study to orchard trees, the crop sub-model should be adapted in future works to consider other parameters such as the height, number and angles of branches, or leaf density. In addition, the possible effects of air or soil temperature variations due to the integration of PV technology should be investigated in future work by improving the proposed methodology. Moreover, future work will be also focused on different optimization criteria and PV technologies. For instance, it would be desirable to optimize the PV system at seasonal or monthly scale according to different crop growing programmes. In addition, other emerging PV transparent PV technologies such as organic of thin-film should be investigated. Finally, the integration of an economic modelling tool should be considered to maximize the revenues of APV systems for greenhouse applications.

CRediT authorship contribution statement

Eduardo F. Fernández: Conceptualization, Formal analysis, Methodology, Writing – original draft, Writing – review & editing, Resources, Funding acquisition. **Antonio Villar-Fernández:** Conceptualization, Investigation, Visualization, Writing – review & editing. **Jesús Montes-Romero:** Software, Visualization, Data curation. **Laura Ruiz-Torres:** Investigation, Data curation, Writing – review & editing. **Pedro M. Rodrigo:** Investigation, Methodology, Writing – review & editing. **Antonio J. Manzaneda:** Investigation, Writing – review & editing, Resources, Funding acquisition. **Florencia Almonacid:** Investigation, Methodology, Supervision, Writing – original draft, Writing – review & editing, Funding acquisition.

Declaration of Competing Interest

The authors declare that they have no known competing financial interests or personal relationships that could have appeared to influence the work reported in this paper.

Acknowledgements

This work has been partially funded by the project "UltraMicroCPV" (MICINN- Agencia Estatal de Investigación: PID2019-106497RB-I00/AEI/10.13039/501100011033) and by the project NACe-CPV/TE (Junta de Andalucía, PAIDI 2020: P18-RT-1595). E.F. Fernández also thank the Spanish Ministry of Science, Innovation and Universities for the funds received under the "Ramón y Cajal Programme" (RYC-2017-21910). P. M. Rodrigo thanks the Spanish Ministry of Science, Innovation and Universities because of the 2020–2024 Beatriz Galindo fellowship (BEAGAL18/00164). Technical and human support provided by Centro de Instrumentación CientíficoTécnica (CICT) of the Universidad de Jaén is gratefully acknowledged.

Annex

Table S 1. Experimental coefficients and determination parameter (R^2) for each crop under consideration.

Family	Species (common name)	a_0	a_1	a_2	a_3	a_4	R^2
Cucurbitaceae	*Citrullus lanatus* Schrad. (Watermelon)	-9.91E-02	3.33E-02	-3.19E-05	1.26E-08	-1.81E-12	0.82
	Cucumis melo L. *(Santa Claus melon)*	-7.68E-01	1.90E-02	-1.86E-05	7.72E-09	-1.10E-12	0.93
	Cucumis melo L. *var. Inodorus (Canary melon)*	-6.79E-01	2.08E-02	-2.07E-05	8.59E-09	-1.23E-12	0.88
	Cucurbita pepo L. *(Zucchini)*	-6.41E-01	2.59E-02	-2.58E-05	1.07E-08	-1.57E-12	0.89
	Cucumis sativus L. (Cucumber)	-1.48E+00	4.06E-02	-4.39E-05	1.96E-08	-3.03E-12	0.97
Fabaceae	*Arachis hypogaea* L. (Peanut)	-4.79E-01	2.80E-02	-1.73E-05	3.52E-09	-1.13E-13	0.89
	Pisum sativum L. *(Pea)*	2.50E-01	2.83E-02	-2.98E-05	1.25E-08	-1.82E-12	0.88
Solanacae	*Capsicum annuum* L. (Pepper)	-1.12E-01	2.96E-02	-3.00E-05	1.19E-08	-1.62E-12	0.93
	Solanum melongena L. (Eggplant)	2.85E-01	2.62E-02	-2.78E-05	1.20E-08	-1.77E-12	0.94
	Solanum lycopersicum Lam. *var.* "Berner Rose" (Berner Rose tomato)	-2.26E-01	3.15E-02	-3.24E-05	1.36E-08	-1.83E-12	0.88
	Solanum lycopersicum Lam. *var.* (Green Zebra tomato)	-2.34E-01	3.00E-02	-3.24E-05	1.36E-08	-1.94E-12	0.95
Poaceae	*Brachypodium distachyon* L. (Purple false brome)	-1.96E-01	3.27E-02	-3.05E-05	1.32E-08	-2.16E-12	0.92
	Brachypodium stacie C. (False brome)	-7.16E-03	4.36E-02	-4.22E-05	1.78E-08	-2.72E-12	0.87
Rosaceae	*Fragaria vesca* L. (Strawberry)	-3.25E-01	3.19E-02	-3.10E-05	1.21E-08	1.67E-12	0.88
	Rubus ideaeus L. (Raspberry)	5.42E-02	3.55E-02	-3.66E-05	1.53E-08	-2.19E-12	0.87

References

[1] Sustainable T, Goals D. The Sustainable Development Goals Report 2020.
[2] IPCC, Assessment Report 6 Climate Change 2021: The Physical Science Basis, (2021). https://www.ipcc.ch/report/ar6/wg1/.
[3] E. Commission, The European Green Deal, (2019).
[4] E. Commission, An EU-wide assessment of National Energy and Climate Plans, (2020).
[5] Nonhebel S. Renewable energy and food supply: Will there be enough land? Renew. Sustain. Energy Rev. 2005;9(2):191–201. https://doi.org/10.1016/j.rser.2004.02.003.
[6] Sills J, Serrano D, Margalida A, Pérez-García JM, Juste J, Traba J, et al. Renewables in Spain threaten biodiversity. Science 2020;370(6522):1282–3.
[7] Hollingsworth JA, Ravishankar E, O'Connor B, Johnson JX, DeCarolis JF. Environmental and economic impacts of solar-powered integrated greenhouses. J. Ind. Ecol. 2020;24(1):234–47. https://doi.org/10.1111/jiec.12934.
[8] N. Gruda, J. Tanny, Protected crops â□" recent advances, innovative technologies and future challenges, in: Acta Hortic., International Society for Horticultural Science (ISHS), Leuven, Belgium, 2015: pp. 271–278. https://doi.org/10.17660/ActaHortic.2015.1107.37.
[9] Chang J, Wu Xu, Wang Y, Meyerson LA, Gu B, Min Y, et al. Does growing vegetables in plastic greenhouses enhance regional ecosystem services beyond the food supply? Front. Ecol. Environ. 2013;11(1):43–9. https://doi.org/10.1890/100223.
[10] J.M. Costa, E. Heuvelink, Greenhouse Horticulture in China : situation and prospects report on a study tour 11 October - 2 November 2003, 2004.
[11] Wang T, Wu G, Chen J, Cui P, Chen Z, Yan Y, et al. Integration of solar technology to modern greenhouse in China: Current status, challenges and prospect. Renew. Sustain. Energy Rev. 2017;70:1178–88. https://doi.org/10.1016/j.rser.2016.12.020.
[12] G. de E. Ministerio de Agricultura, Pesca y Alimentación, Superficies y producciones anuales de cultivos, (n.d.).
[13] Yano A, Cossu M. Energy sustainable greenhouse crop cultivation using photovoltaic technologies. Renew. Sustain. Energy Rev. 2019;109:116–37. https://doi.org/10.1016/j.rser.2019.04.026.
[14] C. van Rijswick, World Vegetable Map 2018, (n.d.).
[15] U.S.D. of Agriculture, N.A.S. Service, Table 14 . Food Crops Grown Under Protection and Sold : 2019 2017 Census of Agriculture 2019 CHS - State Data 429

Table 14 . Food Crops Grown Under Protection and Sold : 2019 (continued) 430 2019 CHS - State Data 2017 Census of Agriculture, 2019.
[16] G. de México, Datos Abiertos, (2016).
[17] Barbosa G, Gadelha F, Kublik N, Proctor A, Reichelm L, Weissinger E, et al. Comparison of land, water, and energy requirements of lettuce grown using hydroponic vs. Conventional agricultural methods. Int. J. Environ. Res. Public Health. 2015;12(6):6879–91. https://doi.org/10.3390/ijerph120606879.
[18] Ntinas GK, Neumair M, Tsadilas CD, Meyer J. Carbon footprint and cumulative energy demand of greenhouse and open-field tomato cultivation systems under Southern and Central European climatic conditions. J. Clean. Prod. 2017;142: 3617–26. https://doi.org/10.1016/j.jclepro.2016.10.106.
[19] R.H.E. Hassanien, M. Li, W. Dong Lin, Advanced applications of solar energy in agricultural greenhouses, Renew. Sustain. Energy Rev. 54 (2016) 989–1001. https://doi.org/10.1016/j.rser.2015.10.095.
[20] Rocamora MC, Tripanagnostopoulos Y. ASPECTS OF PV/T SOLAR SYSTEM APPLICATION FOR VENTILATION NEEDS IN GREENHOUSES. Acta Hortic. 2006;(719):239–46. https://doi.org/10.17660/ActaHortic.2006.719.26.
[21] Yano A, Tsuchiya K, Nishi K, Moriyama T, Ide O. Development of a Greenhouse Side-ventilation Controller driven by Photovoltaic Energy. Biosyst. Eng. 2007;96 (4):633–41. https://doi.org/10.1016/j.biosystemseng.2006.12.012.
[22] Russo G, Anifantis AS, Verdiani G, Mugnozza GS. Environmental analysis of geothermal heat pump and LPG greenhouse heating systems. Biosyst. Eng. 2014; 127:11–23. https://doi.org/10.1016/j.biosystemseng.2014.08.002.
[23] Xu J, Li Y, Wang RZ, Liu W. Performance investigation of a solar heating system with underground seasonal energy storage for greenhouse application. Energy. 2014;67:63–73. https://doi.org/10.1016/j.energy.2014.01.049.
[24] Cuce E, Harjunowibowo D, Cuce PM. Renewable and sustainable energy saving strategies for greenhouse systems: A comprehensive review. Renew. Sustain. Energy Rev. 2016;64:34–59. https://doi.org/10.1016/j.rser.2016.05.077.
[25] Liu Wen, Liu Luqing, Guan Chenggang, Zhang Fangxin, Li Ming, Lv Hui, et al. A novel agricultural photovoltaic system based on solar spectrum separation. A novel agricultural photovoltaic system based on solar spectrum separation 2018; 162:84–94. https://doi.org/10.1016/j.solener.2017.12.053.
[26] La Notte Luca, Giordano Lorena, Calabrò Emanuele, Bedini Roberto, Colla Giuseppe, Puglisi Giovanni, et al. Hybrid and organic photovoltaics for greenhouse applications. Appl. Energy. 2020;278:115582. https://doi.org/10.1016/j.apenergy.2020.115582.
[27] Barron-Gafford Greg A, Pavao-Zuckerman Mitchell A, Minor Rebecca L, Sutter Leland F, Barnett-Moreno Isaiah, Blackett Daniel T, et al. Agrivoltaics provide mutual benefits across the food–energy–water nexus in drylands. Nat. Sustain. 2019;2(9):848–55. https://doi.org/10.1038/s41893-019-0364-5.
[28] Adeh EH, Good SP, Calaf M, Higgins CW. Solar PV Power Potential is Greatest Over Croplands. Sci. Rep. 2019;9:1–6. https://doi.org/10.1038/s41598-019-47803-3.
[29] Ezzaeri K, Fatnassi H, Wifaya A, Bazgaou A, Gourdo L, Aharoune A, et al. Effects of roof-mounted flexible photovoltaic panels on solar radiation and tomato yield in Canarian greenhouse. Acta Hortic. 2020;(1296):87–92. https://doi.org/10.17660/ActaHortic.2020.1296.12.
[30] Cossu Marco, Murgia Lelia, Ledda Luigi, Deligios Paola A, Sirigu Antonella, Chessa Francesco, et al. Solar radiation distribution inside a greenhouse with south-oriented photovoltaic roofs and effects on crop productivity. Appl. Energy. 2014;133:89–100. https://doi.org/10.1016/j.apenergy.2014.07.070.
[31] Elamri Y, Cheviron B, Lopez JM, Dejean C, Belaud G. Water budget and crop modelling for agrivoltaic systems: Application to irrigated lettuces. Agric. Water Manag. 2018;208:440–53. https://doi.org/10.1016/j.agwat.2018.07.001.
[32] Toledo Carlos, Scognamiglio Alessandra. Agrivoltaic systems design and assessment: A critical review, and a descriptive model towards a sustainable landscape vision (three-dimensional agrivoltaic patterns). Sustain. 2021;13(12): 6871. https://doi.org/10.3390/su13126871.
[33] Kadowaki Masayuki, Yano Akira, Ishizu Fumito, Tanaka Toshihiko, Noda Shuji. Effects of greenhouse photovoltaic array shading on Welsh onion growth. Biosyst. Eng. 2012;111(3):290–7. https://doi.org/10.1016/j.biosystemseng.2011.12.006.
[34] Valle B, Simonneau T, Sourd F, Pechier P, Hamard P, Frisson T, et al. Increasing the total productivity of a land by combining mobile photovoltaic panels and food crops. Appl. Energy. 2017;206:1495–507. https://doi.org/10.1016/j.apenergy.2017.09.113.
[35] Marucci A, Cappuccini A. Dynamic photovoltaic greenhouse : Energy balance in completely clear sky condition during the hot period. Energy. 2016;102:302–12. https://doi.org/10.1016/j.energy.2016.02.053.
[36] Hassanien RHE, Li M, Yin F. The integration of semi-transparent photovoltaics on greenhouse roof for energy and plant production. Renew. Energy. 2018;121: 377–88. https://doi.org/10.1016/j.renene.2018.01.044.
[37] Willockx B, Herteleer B, Cappelle J. Techno-economic study of agrovoltaic systems focusing on orchard crops. 37th EU PVSEC. 2020. https://doi.org/10.4229/EUPVSEC20202020-6DO.14.2.
[38] Majumdar D, Pasqualetti MJ. Dual use of agricultural land: Introducing 'agrivoltaics' in Phoenix Metropolitan Statistical Area, USA. Landsc. Urban Plan. 2018;170:150–68. https://doi.org/10.1016/j.landurbplan.2017.10.011.
[39] Weselek Axel, Ehmann Andrea, Zikeli Sabine, Lewandowski Iris, Schindele Stephan, Högy Petra. Agrophotovoltaic systems: applications, challenges, and opportunities. A review. Agron. Sustain. Dev. 2019;39(4). https://doi.org/10.1007/s13593-019-0581-3.
[40] Trommsdorff Max, Kang Jinsuk, Reise Christian, Schindele Stephan, Bopp Georg, Ehmann Andrea, et al. Combining food and energy production: Design of an agrivoltaic system applied in arable and vegetable farming in Germany. Renew. Sustain. Energy Rev. 2021;140:110694. https://doi.org/10.1016/j.rser.2020.110694.
[41] Sekiyama Takashi, Nagashima Akira. Solar sharing for both food and clean energy production: Performance of agrivoltaic systems for corn, a typical shade-intolerant crop. Environ. - MDPI. 2019;6(6):65. https://doi.org/10.3390/environments6060065.
[42] Gonocruz Ruth Anne, Nakamura Ren, Yoshino Kota, Homma Masaru, Doi Tetsuya, Yoshida Yoshikuni, et al. Analysis of the rice yield under an agrivoltaic system: A case study in Japan. Environ. - MDPI. 2021;8(7):65. https://doi.org/10.3390/environments8070065.
[43] C. Baxevanou, D. Fidaros, N. Katsoulas, E. Mekeridis, C. Varlamis, A. Zachariadis, S. Logothetidis, Simulation of Radiation and Crop Activity in a Greenhouse Covered with Semitransparent Organic Photovoltaics, (n.d.).
[44] Edouard S, Combes D, Van Iseghem M, Ng M, Tin W. How does STICS crop model simulate alfalfa productivity in agrivoltaic condition ?, Agrivoltaics 2021 Conf. Exhib. 2021:3–4.
[45] Lee Kangmin, Um Han-Don, Choi Deokjae, Park Jeonghwan, Kim Namwoo, Kim Hyungwoo, et al. The Development of Transparent Photovoltaics. Cell Reports Phys. Sci. 2020;1(8):100143. https://doi.org/10.1016/j.xcrp.2020.100143.
[46] Wu Bo-Sen, Rufyikiri Anne-Sophie, Orsat Valérie, Lefsrud Mark G. Re-interpreting the photosynthetically action radiation (PAR) curve in plants. Plant Sci. 2019;289: 110272. https://doi.org/10.1016/j.plantsci.2019.110272.
[47] De Soto W, Klein SA, Beckman WA. Improvement and validation of a model for photovoltaic array performance. Improvement and validation of a model for photovoltaic array performance 2006;80(1):78–88. https://doi.org/10.1016/j.solener.2005.06.010.
[48] ASTM G173 - 03(2020) Standard Tables for Reference Solar Spectral Irradiances: Direct Normal and Hemispherical on 37° Tilted Surface, (n.d.).
[49] McCree KJ. The action spectrum, absorptance and quantum yield of photosynthesis in crop plants. Agric. Meteorol. 1971;9:191–216. https://doi.org/10.1016/0002-1571(71)90022-7.
[50] Green Martin A, Dunlop Ewan D, Hohl-Ebinger Jochen, Yoshita Masahiro, Kopidakis Nikos, Ho-Baillie Anita WY. Solar cell efficiency tables (Version 55). Prog. Photovoltaics Res. Appl. 2020;28(1):3–15. https://doi.org/10.1002/pip.3228.
[51] Farquhar GD, von Caemmerer S, Berry JA. A biochemical model of photosynthetic CO2 assimilation in leaves of C3 species. Planta 1980;149(1):78–90. https://doi.org/10.1007/BF00386231.
[52] Scholthof Karen-Beth G, Irigoyen Sonia, Catalan Pilar, Mandadi Kranthi K. Brachypodium: A monocot grass model genus for plant biology. Plant Cell. 2018;30 (8):1673–94. https://doi.org/10.1105/tpc.18.00083.
[53] M.C. Peel, B.L. Finlayson, T.A. Mcmahon, Updated world map of the K¨oppen-Geiger climate classification, (2007) 1633–1644.
[54] Valera DL, Belmonte LJ, Molina-Aiz FD, López A, Camacho F. The greenhouses of Almería. Acta Hortic. 2017;(1170):219–26. https://doi.org/10.17660/ActaHortic.2017.1170.25.
[55] Testa R, di Trapani AM, Sgroi F, Tudisca S. Economic sustainability of Italian greenhouse cherry tomato. Sustain. 2014;6:7967–81. https://doi.org/10.3390/su6117967.
[56] Ozkan Burhan, Kurklu Ahmet, Akcaoz Handan. An input-output energy analysis in greenhouse vegetable production: A case study for Antalya region of Turkey. Biomass Bioenergy 2004;26(1):89–95. https://doi.org/10.1016/S0961-9534(03)00080-1.
[57] C. Gueymard, SMARTS2 , A Simple Model of the Atmospheric Radiative Transfer of Sunshine : Algorithms and performance assessment, (1995).
[58] Gueymard CA. The SMARTS spectral irradiance model after 25 years: New developments and validation of reference spectra. Sol. Energy. 2019;187:233–53. https://doi.org/10.1016/j.solener.2019.05.048.
[59] Fernández Eduardo F, Soria-Moya Alberto, Almonacid Florencia, Aguilera Jorge. Comparative assessment of the spectral impact on the energy yield of high concentrator and conventional photovoltaic technology. Sol. Energy Mater. Sol. Cells. 2016;147:185–97. https://doi.org/10.1016/j.solmat.2015.12.003.
[60] Fernández Eduardo F, Talavera DL, Almonacid Florencia M, Smestad Greg P. Investigating the impact of weather variables on the energy yield and cost of energy of grid-connected solar concentrator systems. Energy. 2016;106:790–801. https://doi.org/10.1016/j.energy.2016.03.060.
[61] Rodrigo PM, Fernández EF, Almonacid FM, Pérez- PJ. Solar Energy Materials & Solar Cells Quanti fi cation of the spectral coupling of atmosphere and photovoltaic system performance : Indexes, methods and impact on energy harvesting. Sol. Energy Mater. Sol. Cells. 2017;163:73–90. https://doi.org/10.1016/j.solmat.2017.01.018.
[62] Solas AF, Micheli L, Almonacid F, Fernandez EF. Comparative Analysis of Methods to Extract Soiling Losses: Assessment with Experimental Measurements, in. Conf. Rec. IEEE Photovolt. Spec. Conf. 2021:160–4. https://doi.org/10.1109/PVSC43889.2021.9518699.
[63] Bessa João Gabriel, Micheli Leonardo, Almonacid Florencia, Fernández Eduardo F. Monitoring photovoltaic soiling: assessment, challenges, and perspectives of current and potential strategies. IScience. 2021;24(3):102165. https://doi.org/10.1016/j.isci.2021.102165.
[64] Yildirim N, Bilir L. Evaluation of a hybrid system for a nearly zero energy greenhouse. Energy Convers. Manag. 2017;148:1278–90. https://doi.org/10.1016/j.enconman.2017.06.068.